Available online at www.sciencedirect.com
ScienceDirect
Journal of Power Sources 175 (2008) 540–546
JOURNAL OF POWER SOURCES
www.elsevier.com/locate/jpowsour

Interfacial reactions between graphite electrodes and propylene carbonate-based solutions: Electrolyte-concentration dependence of electrochemical lithium intercalation reaction

Soon-Ki Jeong [a,*], Minoru Inaba [b], Yasutoshi Iriyama [c], Takeshi Abe [c], Zempachi Ogumi [c]

[a] *Department of Chemical Engineering, Soonchunhyang University, Asan, Chungnam 336-745, Republic of Korea*
[b] *Department of Molecular Science and Technology, Faculty of Engineering, Doshisha University, Kyotanabe, Kyoto 610-0321, Japan*
[c] *Department of Energy & Hydrocarbon Chemistry, Graduate School of Engineering, Kyoto University, Nishikyo-ku, Kyoto 615-8510, Japan*

Received 29 May 2007; received in revised form 7 August 2007; accepted 10 August 2007
Available online 1 September 2007

Abstract

This study examines the electrochemical reactions occurring at graphite negative electrodes of lithium-ion batteries in a propylene carbonate (PC) electrolyte that contains different concentrations of lithium salts such as, $LiClO_4$, $LiPF_6$ or $LiN(SO_2C_2F_5)_2$. The electrode reactions are significantly affected by the electrolyte concentration. In concentrated solutions, lithium ions are reversibly intercalated within the graphite to form stage 1 lithium–graphite intercalation compounds (Li–GICs), regardless of the lithium salt used. On the other hand, electrolyte decomposition and exfoliation of the graphene layers occur continuously in the low-concentration range. *In situ* analysis with atomic force microscopy reveals that a thin film (thickness of ~8 nm) forms on the graphite surface in a concentrated solution, e.g., 3.27 mol kg^{-1} $LiN(SO_2C_2F_5)_2$/PC, after the first potential cycle between 2.9 and 0 V *versus* Li^+/Li. There is no evidence of the co-intercalation of solvent molecules in the concentrated solution.

Keywords: Graphite negative electrode; Propylene carbonate; Lithium intercalation; Atomic force microscopy; Surface film

1. Introduction

The invention of the lithium-ion battery has been one of the most significant advances in electrochemical energy-storage technology. These batteries store the highest amount of energy per unit mass among the various types of rechargeable battery, and are widely employed in portable electronic devices. In commercially available lithium-ion batteries, graphite has been used as the negative electrode on account of its relatively high specific reversible capacity (theoretically 372 mAh g^{-1}), small irreversible capacity, and good cycleability [1,2]. Graphite has a layer structure that reversibly accepts lithium ions between its layers during charging (lithium intercalation) and releases them during discharging (lithium de-intercalation). These electrochemical reactions at the graphite negative electrodes occur at potentials <0.25 V *versus* Li^+/Li. At such potentials, aqueous solutions cannot be used as electrolytes because of excessive hydrogen gas evolution. Therefore, non-aqueous organic solutions have been used as an electrolyte. The typical liquid electrolyte solutions for lithium-ion batteries are ethylene carbonate (EC)-based solutions containing lithium salts such as $LiClO_4$, $LiPF_6$, $LiBF_4$, etc. In the field of lithium-ion battery technology, EC has been a solvent of great importance because the lithium intercalation and de-intercalation reactions at graphite electrodes are highly reversible in EC-based solutions. The development of EC-based solutions has allowed the use of graphite as the negative electrode in commercial lithium-ion batteries [3].

On the other hand, there has been considerable research on propylene carbonate (PC)-based solutions [4–10]. One of the major reasons for the interest in these solutions is that they exhibit superior ionic conductivity to EC-based solutions at low temperatures [11]. Prior to the introduction of EC-based solutions, early attempts to intercalate lithium within graphite had been performed in PC-based solutions, but without success [12–15]. When graphite electrodes were taken to

* Corresponding author. Tel.: +82 41 530 1313; fax: +82 41 530 1313.
E-mail address: hamin611@sch.ac.kr (S.-K. Jeong).

0378-7753/$ – see front matter © 2007 Published by Elsevier B.V.
doi:10.1016/j.jpowsour.2007.08.065

negative potentials in PC-based solutions, electrolyte decomposition and exfoliation of graphene layers occurred instead of lithium intercalation. It is generally accepted that the different electrochemical behaviour of graphite between EC- and PC-based solutions is the result of the film-forming ability of the electrolyte solution. EC provides a surface film on a graphite electrode as a result of its reductive decomposition upon the initial charging. This film suppresses further electrolyte decomposition as well as the co-intercalation of solvent molecules quite effectively, and thereby allows only lithium-ion migration. This feature is not, however, observed with PC. Many researchers have investigated means to provide an effective surface film on graphite in PC-based solutions. As a consequence, various types of film-forming agent have been suggested, e.g., chloroethylene carbonate [4,5], 12-crown-4 [6], vinylene carbonate [7], ethylene sulfite [8], fluoroethlyene carbonate [9], dimethylsulfoxide [10]. By adding one of these to the electrolyte solution, the film-forming problems caused by the use of pure PC as a solvent have been overcome to a considerable extent.

Recently, we reported that lithium ions were intercalated within graphite to form a stage 1 lithium–graphite intercalation compound (Li–GIC) in a PC-based solution containing none of the film-forming agents described above, i.e., 2.72 mol dm^{-3} $LiN(SO_2C_2F_5)_2$/PC [16]. This result showed that the poor compatibility between graphite and PC could be improved without the need for a film-forming agent. Nevertheless, the concentration of an electrolyte solution is also an important factor for obtaining Li–GICs from PC-based solutions. Accordingly, this study examines the effects of electrolyte concentration on the interfacial reactions between graphite and PC-based solutions (with no film-faming agents) during charging and discharging.

2. Experimental

The electrolyte solutions were prepared by dissolving a lithium salt such as $LiClO_4$, $LiPF_6$ or $LiN(SO_2C_2F_5)_2$ in PC or in a 1:1 (by volume) mixture of EC and diethyl carbonate (DEC) (EC + DEC). All these reagents were purchased from Kishida Chemical Co. and were used as-received. The water content in each solution was <30 ppm, which was confirmed by means of a Karl–Fischer moisture titrator (Kyoto Electronics Manufacturing Co., MKC-210).

Natural graphite powder (The Kansai Coke and Chemicals Co., NG-7) was used for the charge and discharge tests. The test electrode was prepared by coating a mixture of the graphite powder and the polymeric binder on copper foil, as described elsewhere [17]. The charge and discharge tests were conducted with conventional three-electrode cells at a constant current of 2.2 mA g^{-1}. Lithium foil was used for both the counter and reference electrodes. In some experiments, the fully charged graphite electrodes were removed from the test cells and mounted in a sealed holder with a beryllium window for structural analysis by X-ray diffraction (XRD). The XRD data were collected with a Rigaku RINT 2200 diffractometer equipped with a Cu Kα source (40 kV, 40 mA).

A highly oriented, pyrolytic graphite (HOPG) block (Advanced Ceramics, ZYH grade) was used for atomic force microscopy (AFM) observations. A flat surface was easily prepared by cleaving the HOPG. The *in situ* electrochemical AFM observations were performed in a conventional contact mode using an AFM system (Molecular Imaging, PicoSPM) equipped with a potentiostat (Molecular Imaging, PicoStat) and a laboratory-made electrochemical cell. The freshly cleaved HOPG was mounted on the bottom of the cell. Only the basal plane was brought into contact with the electrolyte solution by means of an O-ring. The geometric surface area was 1.2 cm^2. The counter and reference electrodes were lithium foil. Pyramidal silicon nitride tips were used for the AFM measurements. Cyclic voltammetry (CV) was performed between 2.9 and 0.0 V at a sweep rate of 0.5 mV s^{-1}. The AFM images were obtained continuously at an interval of 150 mV during the CV measurements.

All electrochemical measurements, including AFM, were carried out in an argon-filled glove-box (Miwa, MDB-1B + MM3-P60S) with a dew point <−60 °C. All potentials are reported as volts *versus* Li^+/Li. The concentration of all electrolyte solutions is expressed as the molality of lithium salt (mol kg^{-1}).

3. Results and discussion

3.1. Electrochemical lithium intercalation within graphite from PC-based solutions

The potential profiles of the natural graphite powder (NG-7) during the first charging and discharging cycle in PC containing different $LiN(SO_2C_2F_5)_2$ concentrations are given in Fig. 1. At concentrations ranging from 1.23 to 2.45 mol kg^{-1}, the potential of the graphite electrodes falls rapidly during charging and then remains almost constant between 0.9 and 0.8 V, as shown in Fig. 1(a). This suggests that electrolyte decomposition and the exfoliation of graphene layers occur continuously at the graphite electrodes, as has been reported in the literature [13,18]. It is a well-known fact that the electrochemical intercalation of lithium into graphite is accompanied a series of potential plateaux, which correspond to reversible transformations between the different-staged structures of Li–GICs depending on the lithium concentration, at potentials <0.25 V [1,2]. There are no potential plateaux in Fig. 1(a), however, which indicates that lithium is not intercalated into graphite from 1.23 to 2.45 mol kg^{-1} solutions. By contrast, the potentials dropped to <0.25 V in 3.27 and 4.90 mol kg^{-1} solutions, as shown in Fig. 1(b), and potential plateaux appeared on the charge and discharge curves. These potential profiles show that lithium ions are reversibly intercalated into, and de-intercalated from, the graphite in the two solutions to form Li–GICs. The potential profiles are similar to those observed in the EC-based solutions, and the specific discharge capacities (364 and 355 mAh g^{-1} in 3.27 and the 4.90 mol kg^{-1} solutions, respectively) are comparable with those obtained in EC-based solutions [1,2]. These results clearly indicate that the electrochemical lithium intercalation reaction at the graphite electrode is greatly affected by the $LiN(SO_2C_2F_5)_2$ concentration. Such an electrolyte-concentration dependence of the lithium intercalation reaction

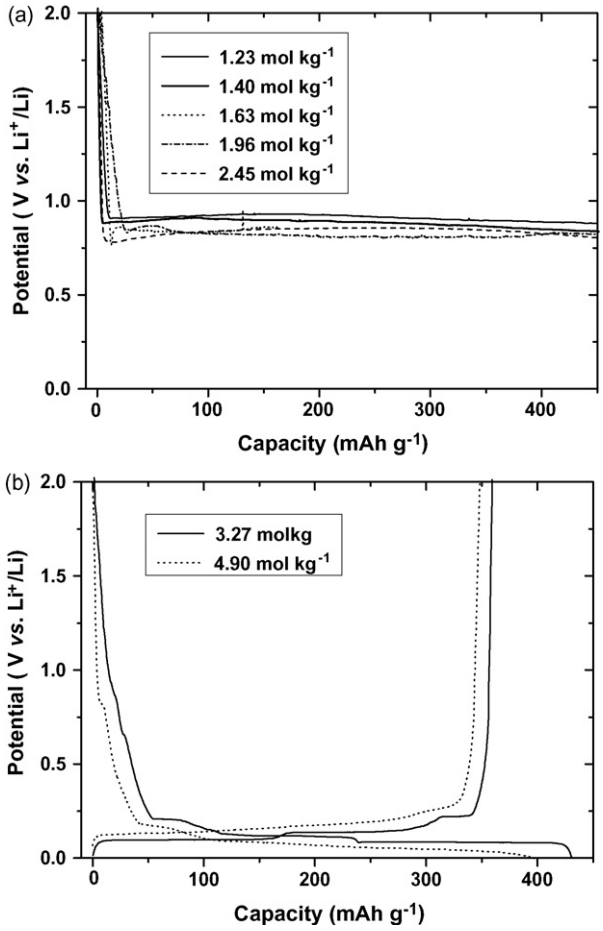

Fig. 1. Charge and discharge curves for first cycle of natural graphite powder (NG-7) in PC containing relatively (a) low-concentrations of $LiN(SO_2C_2F_5)_2$ and (b) high-concentrations of $LiN(SO_2C_2F_5)_2$.

is also observed in $LiClO_4$/PC and $LiPF_6$/PC solutions. Lithium ions are intercalated within the graphite to form Li–GICs in the high-concentration solutions, i.e., $\geq$3.27 mol kg^{-1} $LiClO_4$/PC and $\geq$2.45 mol kg^{-1} $LiPF_6$/PC (see Fig. 2). Li–GICs are not, however, formed in lower-concentration solutions.

3.2. Structural analysis of Li–GICs formed in PC-based solutions

Fig. 2 shows the XRD patterns of a pristine graphite electrode and Li–GICs obtained from the above-mentioned concentrated PC-based solutions by charging to 0 V. Fig. 2(b) shows the XRD pattern of a Li–GIC obtained from an EC-based solution, e.g., 0.91 mol kg^{-1} $LiClO_4$/EC + DEC, for comparison. The layer structure of graphite leads to a strong (0 0 2) reflection, which appears at 26.5° from the pristine graphite electrode (Fig. 2(a)). Lithium intercalation between the graphene layers results in an expansion of the interlayer spacing, and consequently, a shift in the (0 0 2) peak to a lower angle. The XRD pattern in Fig. 2(b) is typical of a stage 1 Li–GIC; the large peak at 24.2° and a small peak at 49.3° correspond to the (0 0 1) and (0 0 2) planes, respectively [19–21]. XRD patterns similar to that shown in Fig. 2(b) are obtained for graphite electrodes when fully charged in 3.27 mol kg^{-1} $LiN(SO_2C_2F_5)_2$/PC, 3.27 mol kg^{-1} $LiClO_4$/PC and 2.45 mol kg^{-1} $LiPF_6$/PC electrolytes, as indicated in Fig. 1(c)–(e), respectively. From these data, it is concluded that stage 1 Li–GICs are formed in the three PC-based solutions.

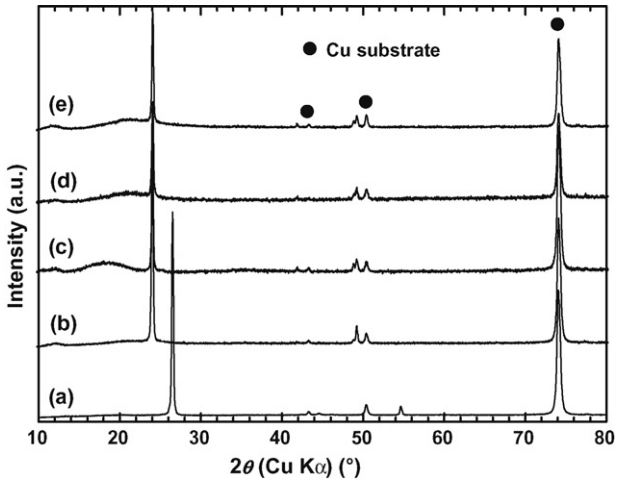

Fig. 2. XRD patterns of graphite electrodes (a) before and (b–e) after the first charging in (b) 0.91 mol kg^{-1} $LiClO_4$/EC + DEC (1:1), (c) 3.27 mol kg^{-1} $LiN(SO_2C_2F_5)_2$/PC, (d) 3.27 mol kg^{-1} $LiClO_4$/PC and (e) 2.45 mol kg^{-1} $LiPF_6$/PC.

3.3. In situ observation of surface film formation

The above results (charge–discharge curves, XRD patterns) provide new insights into the electrochemical preparation of Li–GICs. It is found that lithium intercalation within graphite from the PC-based solutions is an electrochemical reaction that is strongly dependent on the electrolyte concentration. Li–GICs are not formed in relatively low-concentration PC-based solutions, i.e., the lithium intercalation reaction does not take place on the graphite electrode. Although many researchers have reported a poor compatibility between graphite and PC, the situation can be improved significantly by increasing the electrolyte concentration. When the electrolyte concentration reaches at a certain point, lithium ions began to intercalate within the graphite to form Li–GICs despite the use of pure PC as a solvent. The electrolyte solutions do not contain any film-forming agents. This suggests that the concentrated PC-based solutions produced an effective surface film on the graphite electrode without the need for film-forming agents.

Detail information on the formation of the surface film in concentrated PC-based solutions was obtained by monitoring the changes in morphology of the HOPG basal plane with AFM during a slow CV scan. The HOPG was used as a model of the composite graphite negative electrodes employed in the charge–discharge test. Fig. 3 shows cyclic voltammograms of the HOPG basal plane between 2.9 and 0.0 V at 0.5 mV s^{-1} in 3.27 mol kg^{-1} $LiN(SO_2C_2F_5)_2$/PC. Two small reduction peaks, centred at 2.05 and 0.75 V, appear in the first cycle but disappear in the second. This means that they are the result of irreversible electrolyte decomposition, which is closely related to surface

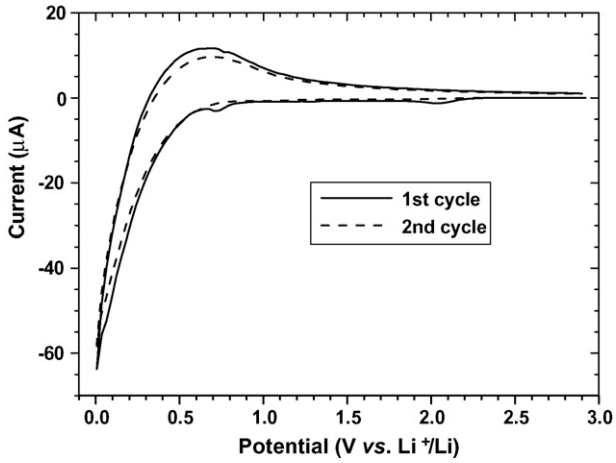

Fig. 3. Cyclic voltammograms of HOPG basal plane in 3.27 mol kg^{-1} $LiN(SO_2C_2F_5)_2$/PC. Sweep rate: 0.5 mV s^{-1}.

film formation. In addition to the two small reduction peaks, a large reduction peak is observed at a potential close to 0 V, and a broad oxidation peak is present between 0.4 and 1.0 V on the first cycle. These two peaks can be assigned to lithium intercalation and de-intercalation, respectively. It is believed, however, that the reduction peak involves a large proportion of the irreversible electrolyte decomposition reaction because the charge consumed is still greater than that consumed for oxidation.

Fig. 4 presents the changes in morphology of the HOPG basal plane obtained simultaneously during the first cyclic voltammogram shown in Fig. 3. An AFM image obtained at 2.9 V before potential cycling is given in Fig. 4(a). The surface consists of atomically flat terraces that are separated by several steps. These features represent the typical surface structure of the HOPG basal plane. At this potential, the HOPG surface is quite inert, and neither deposition nor intercalation occurs. The same area shown in Fig. 4(a) was imaged during the CV measurement, the micrograph obtained over the potential range of 0.95–0.80 V are presented in Fig. 4(b). The arrow in parenthesis denotes the direction of the raster-scan, i.e., the bottom and the top scanning lines were obtained at 0.95 and 0.80 V, respectively. The changes in morphology begin at around 0.85 V, and particle-like precipitates appear on the HOPG surface. This is well correlated with the reduction peak that is centred at 0.75 V on the first cycle shown in Fig. 3. The precipitates are the irreversible decomposition products of the electrolyte solution. Although a

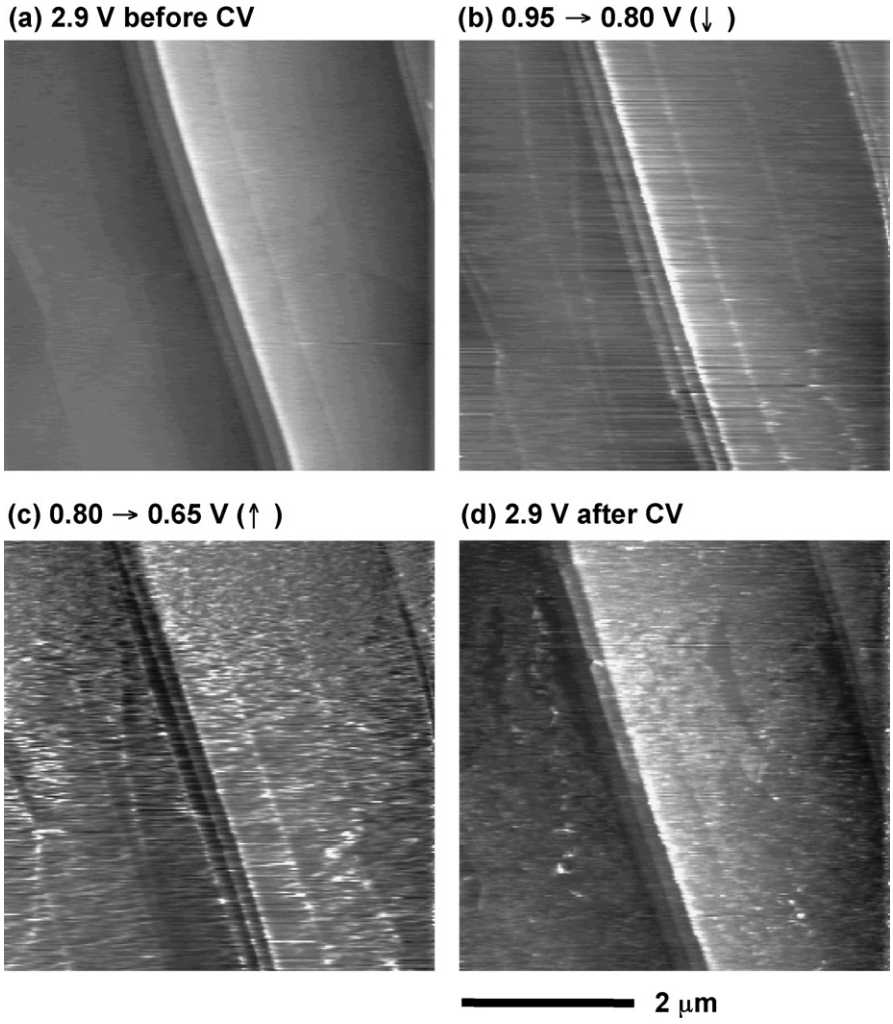

Fig. 4. AFM images (5 μm × 5 μm) of HOPG basal plane surface obtained (a) before CV, (b and c) during first CV cycle and (d) after CV at 0.5 mV s^{-1} in 3.27 mol kg^{-1} $LiN(SO_2C_2F_5)_2$/PC.

small reduction current flows at approximately 2.05 V in Fig. 3, no morphological changes are observed. This suggests that the reaction products formed at 2.05 V are highly soluble in the electrolyte solution. As shown in Fig. 4(c), the number of precipitates increases with decreasing potential, and the whole HOPG surface becomes covered with precipitates. These precipitates are insoluble in the electrolyte solution and remain on the HOPG surface after the first cycle, as shown in Fig. 4(d). This means that the precipitates serve as an effective surface film.

It has been reported [22–26] that two irreversible reactions have to be suppressed in order to obtain Li–GIC in non-aqueous solutions using the electrochemical method, namely: solvent co-intercalation into the edge plane and direct electrolyte decomposition on the basal and edge planes. Although these irreversible reactions are inevitable during initial charging, the amount of charge consumed therein depends greatly on the chosen electrolyte solution. It is understandable that the irreversible reactions are suppressed in the 3.27 mol kg^{-1} $LiN(SO_2C_2F_5)_2$/PC used in the above CV and AFM measurements because the lithium ions are reversibly intercalated within graphite in the solution to form stage 1 Li–GIC, as mentioned earlier.

3.4. Properties of surface film formed on HOPG

After the first cycle of CV was completed, AFM scanning was continued at 2.9 V, where no electrode reactions take place, and images were collected for each scan; some examples are given in Fig. 5. A few irregular-shaped holes develop on the HOPG surface after the 50th scan; see Fig. 5(a). It is obvious that these holes are formed at places where the precipitates have been removed. With repeated scanning (50 → 85 → 100 → 120 cycles), the number and size of the holes increases gradually. After the 120th scan (Fig. 5(d)), a larger number of precipitates have disappeared from the scanned area. This phenomenon is attributed to surface scraping due to the AFM tip. As mentioned in Section 2, the AFM observations in this study were carried out in contact mode, in which the tip is in contact with the sample surface during the entire measurement. It is known that this procedure is capable of scraping materials that are weakly attached to the sample surface [27–31]. Therefore, it is reasonable to conclude that the precipitates shown in Fig. 4(d) were dragged by the AFM tip from their original location and deposited at the edge of the scan area during the repeated scanning, which results in the significant changes in morphology observed in Fig. 5. Similar surface-scraping phenomena have been observed in the previous

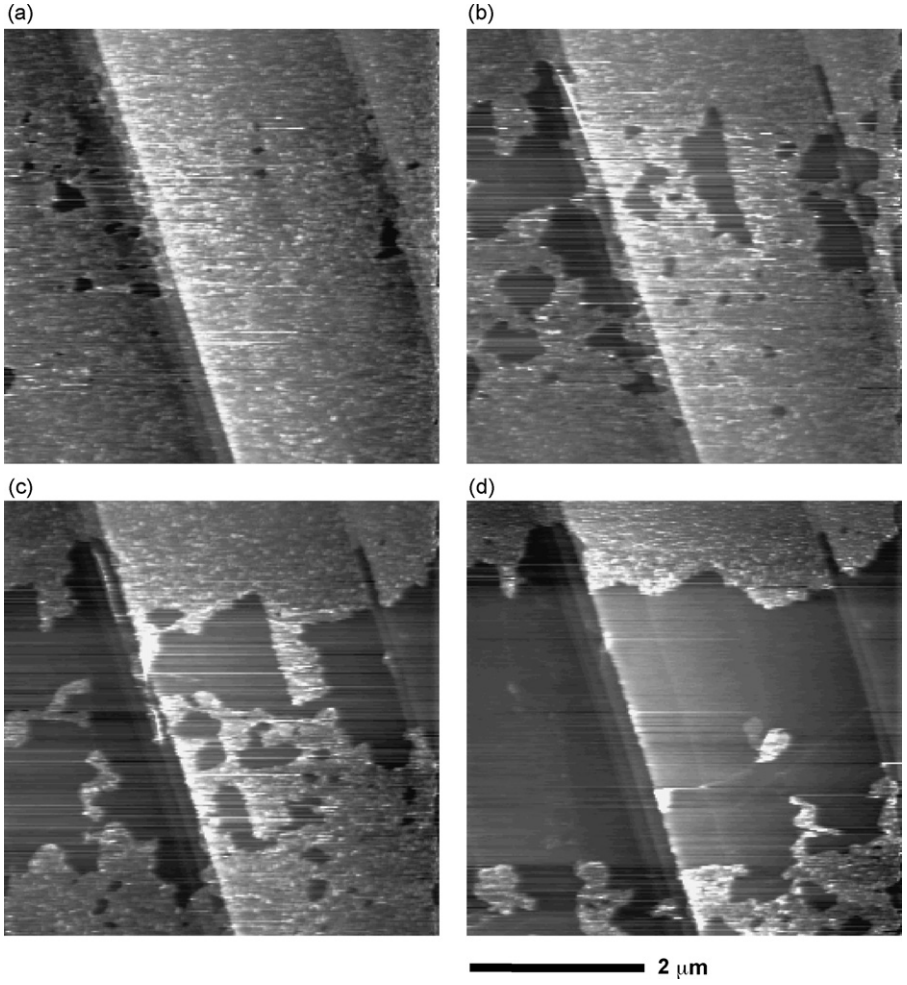

Fig. 5. AFM images (5 μm × 5 μm) of HOPG basal plane surface obtained at 2.9 V after the first cycle of CV at 0.5 mV s^{-1} in 3.27 mol kg^{-1} $LiN(SO_2C_2F_5)_2$/PC. Each image was obtained at (a) 50, (b) 85, (c) 100 and (d) 120th AFM scans.

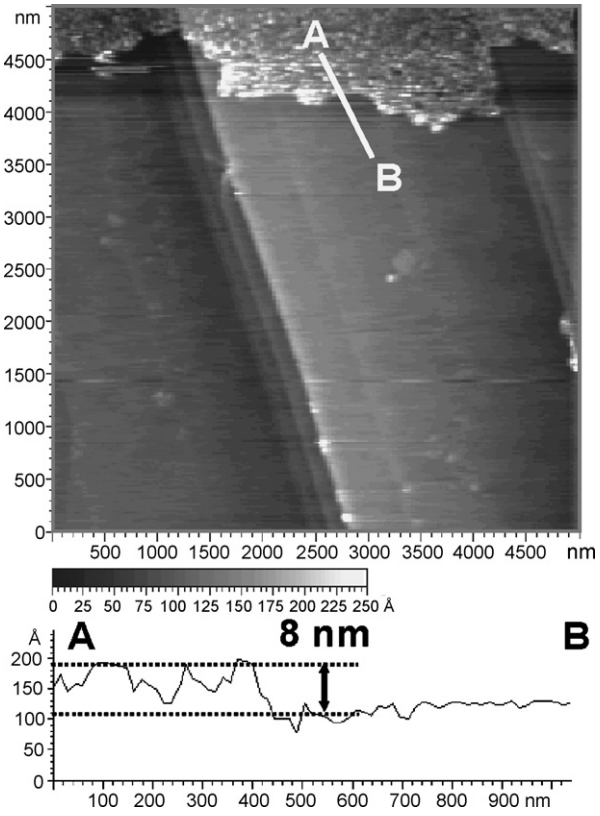

Fig. 6. AFM image (5 μm × 5 μm) and height profile of HOPG basal plane surface obtained at 2.9 V after 170 AFM scans after first CV cycle at 0.5 mV s^{-1} in 3.27 mol kg^{-1} $LiN(SO_2C_2F_5)_2$/PC.

in situ AFM studies [17,24–26,32,33]. Although AFM analysis does not provide direct information on the chemical composition of a sample, the surface-scraping phenomenon shown in Fig. 5 suggests that the precipitates formed on HOPG are soft materials such as polymers [34,35].

After the 180th scan, almost all the precipitates except those formed on the top part of the scan area are removed; see Fig. 6. From the height profile, the thickness of the precipitate layer is approximately 8 nm. This value is much smaller than that obtained in EC-based solutions, in which relatively thick precipitate layers (16–40 nm of height) are formed on a HOPG surface, as shown in our earlier studies [24,25]. Another notable feature from Fig. 6 is that there is no evidence of solvent co-intercalation on the surface, i.e., at where the precipitate layer had been removed by multiple scans. In previous studies, it was found that when a graphite electrode was taken to a negative potential, solvent molecules and lithium ions were intercalated within the graphite. These then decomposed between the graphene layers and gave rise to, exfoliation of the layers or large swelling (blisters) of 20–100 nm in height [24,25]. The image in Fig. 6 shows that there is no exfoliation and swelling. Therefore, the solvent co-intercalation reaction has not taken place at the HOPG electrode during potential cycling in the 3.27 mol kg^{-1} $LiN(SO_2C_2F_5)_2$/PC electrolyte. This means that the precipitate layer shown in Fig. 4(d) plays a role in suppressing both solvent co-intercalation into the edge plane and direct electrolyte decomposition on the basal and edge planes.

4. Conclusion

Lithium intercalation within graphite from PC-based solutions is an electrochemical reaction that strongly depends on the electrolyte concentration, and PC is a good film-forming agent. In concentrated PC-based solutions, lithium ions are intercalated electrochemically into the graphite electrode to form stage 1 Li–GIC whereas no solvent decomposition or the intensive exfoliation of graphene layers occurs in the relatively low-concentration solutions. The graphite electrode showed a good reversible charge–discharge behaviour in concentrated PC-based solutions similar to that observed in EC-based solutions. *In situ* electrochemical AFM studies have provided valuable information on surface film formation in 3.27 mol kg^{-1} $LiN(SO_2C_2F_5)_2$/PC solution. This solution produces a very thin surface film (thickness of ∼8 nm) on graphite. The surface film suppresses both the co-intercalation of PC molecules between the graphene layers and further electrolyte decomposition on the graphite surface. Although the detailed mechanism of the different surface films formed according to the electrolyte concentration is unclear, these results suggest that the electrolyte concentration is an important factor that determines the performance of a surface film on a graphite electrode.

References

[1] Z. Ogumi, M. Inaba, Bull. Chem. Soc. Jpn. 71 (1998) 521.
[2] M. Winter, J.O. Besenhard, M.E. Spahr, P. Novak, Adv. Mater. 10 (1998) 725.
[3] R. Fong, U. von Sacken, J.R. Dahn, J. Electrochem. Soc. 137 (1990) 2009.
[4] Z.X. Shu, R.S. McMillan, J.J. Murray, J. Electrochem. Soc. 142 (1995) L161.
[5] A. Naji, P. Willmann, D. Billud, Carbon 36 (1998) 1347.
[6] Z.X. Shu, R.S. McMillan, J.J. Murray, J. Electrochem. Soc. 140 (1993) L101.
[7] P. Biensan, J. M. Bodet, F. Perton, M. Broussely, C. Jehoulet, S. Barusseau, S. Herreyre, B. Simon, Extended Abstracts of the 10th International Meeting on Lithium Batteries, Como, Italy, Abs. No. 286, 2000.
[8] G.H. Wrodnigg, J.O. Besenhard, M. Winter, J. Electrochem. Soc. 146 (1999) 470.
[9] R. McMillan, H. Slegr, Z.X. Shu, W. Wang, J. Power Sources 81–82 (1999) 20.
[10] T. Abe, Y. Mizutani, N. Kawabata, M. Inaba, Z. Ogumi, Synth. Met. 125 (2002) 249.
[11] J.T. Dudley, D.P. Wilkinson, G. Thomas, R. LeVae, S. Woo, H. Blom, C. Horvath, M.W. Juzkow, B. Denis, P. Juric, P. Aghakian, J.R. Dahn, J. Power Sources 35 (1991) 59.
[12] A.N. Dey, B.P. Sullivan, J. Electrochem. Soc. 117 (1970) 222.
[13] J.O. Besenhard, H.P. Fritz, J. Electroanal. Chem. 53 (1974) 329.
[14] G. Eichinger, J. Electroanal. Chem. 74 (1976) 183.
[15] M. Arakawa, J. Yamaki, J. Electroanal. Chem. 219 (1987) 273.
[16] S.-K. Jeong, M. Inaba, Y. Iriyama, T. Abe, Z. Ogumi, Electrochem. Solid State Lett. 6 (2003) A13.
[17] S.-K. Jeong, M. Inaba, R. Mogi, T. Abe, Z. Ogumi, Langmuir 17 (2001) 8281.
[18] M. Inaba, Z. Siroma, Y. Kawatate, A. Funabiki, Z. Ogumi, J. Power Sources 68 (1997) 221.
[19] J.R. Dahn, Phys. Rev. B 44 (1991) 9170.
[20] T. Ohzuku, Y. Iwakoshi, K. Sawai, J. Electrochem. Soc. 140 (1993) 2490.
[21] Z. Jiang, M. Alamair, K.M. Abraham, J. Electrochem. Soc. 142 (1995) 333.
[22] J.O. Besenhard, M. Winter, J. Yang, W. Biberacher, J. Power Sources 54 (1995) 228.

[23] M. Winter, G.H. Wrodingg, J.O. Besenhard, W. Biberacher, P. Novak, J. Electrochem. Soc. 147 (2000) 2427.
[24] S.-K. Jeong, M. Inaba, T. Abe, Z. Ogumi, J. Electrochem. Soc. 148 (2001) A989.
[25] S.-K. Jeong, M. Inaba, Y. Iriyama, T. Abe, Z. Ogumi, Electrochim. Acta 47 (2002) 1975.
[26] S.-K. Jeong, M. Inaba, Y. Iriyama, T. Abe, Z. Ogumi, J. Power Sources 119–121 (2003) 555.
[27] J. Frommer, W. Heckl, in: R. Colton, A. Engel, J. Frommer, H. Gaub, A. Gewirth, R. Guckenberger, J. Rabe, W. Heckel, B. Parkinson (Eds.), Procedures in Scanning Probe Microscopies, John Wiley & Sons, Chichester, 1998, pp. 277–352.
[28] R.M. Overney, E. Meyer, MRS Bull. 18 (1993) 26.
[29] R.M. Overney, H. Takano, M. Fujihira, E. Meyer, H.-J. Guntherodt, Thin Solid Films 240 (1994) 105.
[30] V.V. Tsukruk, D.H. Reneker, Polymer 36 (1995) 1791.
[31] P. Lemoine, J.M. Laughlin, Thin Solid Films 339 (1999) 258.
[32] M. Inaba, H. Tomiyasu, A. Tasaka, S.K. Jeong, M. Ogumi Z, Langmuir 17 (2004) 8281.
[33] M. Inaba, H. Tomiyasu, A. Tasaka, S.K. Jeong, M. Iriyama, Y. Abe, T. Ogumi Z, Electrochemistry 71 (2003) 1132.
[34] E. Pled, D. Bar-Tow, A. Merson, A. Gladkich, L. Burstein, D. Golodnitsky, J. Power Sources 97–98 (2001) 52.
[35] Z. Ogumi, A. Sano, M. Inaba, T. Abe, J. Power Sources 97–98 (2001) 156.